Thermal and Residual Stress Distribution in Stainless Steel pipe welds: Experiments and Modelling

Niraj Deobhankar, P. K. Singh, V. Bhasin, K. K. Vaze*
Reactor Safety Division, Hall- 7, Bhabha Atomic Research Centre
Mumbai-400 085, India

ABSTRACT

Aim of the present paper is to simulate the austenitic stainless steel weld joints and predict the temperature and residual stress distribution and to compare the predicted results with experiment. In first set, weld bead on plate has been simulated and analysed using finite element method (FEM). The welding process used for bead on plate was gas tungsten arc welding (GTAW). In second set, SS304LN pipe weld joints have been simulated and analysed. These weld joints have been prepared using hot wire GTAW with narrow gap and cold wire GTAW with conventional V-groove. Double ellipsoidal heat source has been used to simulate heat effect of the welding. Heat capacity, thermal conductivity, elastic modulus, yield stress and other material properties have been treated as temperature dependent. Temperature distributions have been predicted from 3D transient analysis considering the effects of conduction, radiation and convection. Residual stress distributions have been predicted from the analysis by incorporating thermo-elasto-plasticity and boundary conditions. On experimental side peak temperature, heating rate and cooling rate have been recorded using thermocouple and data recorder during welding in both sets. Residual stress has been measured using x-ray diffraction technique for bead on plate and blind hole drilling technique for pipe welds. The experimental and numerical analysis results for temperature and residual stress have been compared. The temperature distribution compares well for both cases and residual stress compares well for bead on plate. Predicted residual stress in pipes is on higher side.

INTRODUCTION

Austenitic stainless steel pipe welding using GTAW have been very common in piping system and nuclear power reactor. Welding utilizes concentrated heat sources which result in local melting of the metal. Uneven heating and cooling rate of the component along with constraints during welding lead to generation of residual stresses. These residual stresses are detrimental to the performance of components. Tensile residual stress is known as one of the major component of failure due to stress corrosion cracking.

Thermal analysis of welding was first attempted by Rosenthal [1] in 1946. Double ellipsoidal heat source was introduced by Goldak [2] in 1984 which proved instrumental in prediction of temperature and residual stress distribution. Brickstad and Josefan [3] carried out parametric study of multipass circumferential butt welding of stainless steel pipes using finite element analysis. Dean Dang [4, 5] carried out finite element analysis multipass weld joints for plates as well as pipes. The recent European modelling and measurement round robin exercise conducted as part of the NeT network- Network on neutron techniques standardisation for structural integrity considered a single weld bead on 316L stainless steel plate. The numerical predictions of residual stresses arising from the round robin showed a large scatter, which underlines deficiencies in simulating the welding process among the existing numerical codes [6, 7]. Hence, in this study, simple geometry such as bead on plate was considered in first set. This will help in validating FEM prediction. Thereafter similar procedure can be followed for pipe weld joint.

In this paper, first section describes experimental procedure of GTAW bead on plate of 304LN and pipe girth weld of 304LN stainless steel pipes using GTAW with narrow groove and also conventional groove. Second section deals with finite element methods applied to predict temperature cycle and residual stresses in the plate and pipe weld. Experimental results with FEM predictions were compared in third section of this paper.

EXPERIMENTAL DETAILS

Welding and Temperature Measurement

Experiments have been conducted to record data on temperature distribution with respect to time and measure residual stresses on the bead on plate and the pipe welds. Material used in the study was austenitic stainless steel (SS 304LN). The chemical compositions of the parent material and filler rod are given in the Table 1. A 304LN plate of dimensions 180 X 120 X 20 mm was placed freely on a weld table. Semi-automatic GTAW has been used with filler rod of 2.4 mm diameter to produce a bead of 100 mm length as shown in Fig. 1.

Table 1: Composition of material used in welding

Composition	***C***	***Mn***	***Si***	***S***	***P***	***Cr***	***Ni***	***N***	***Mo***	***Cu***
Content of parent material SS 304LN	0.021	0.79	0.33	0.003	0.004	18.26	8.45	0.10	---	---
Content of Filler material ER 308 L	0.017	1.72	0.37	0.011	0.023	19.88	10.02	---	0.24	0.19

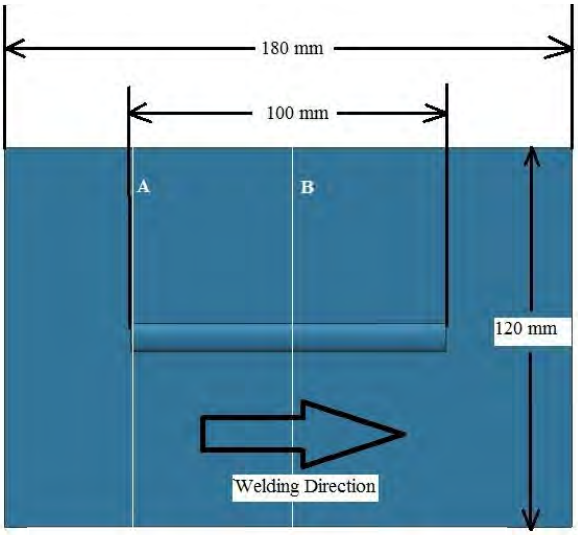

Figure 1: Geometry of Bead on plate

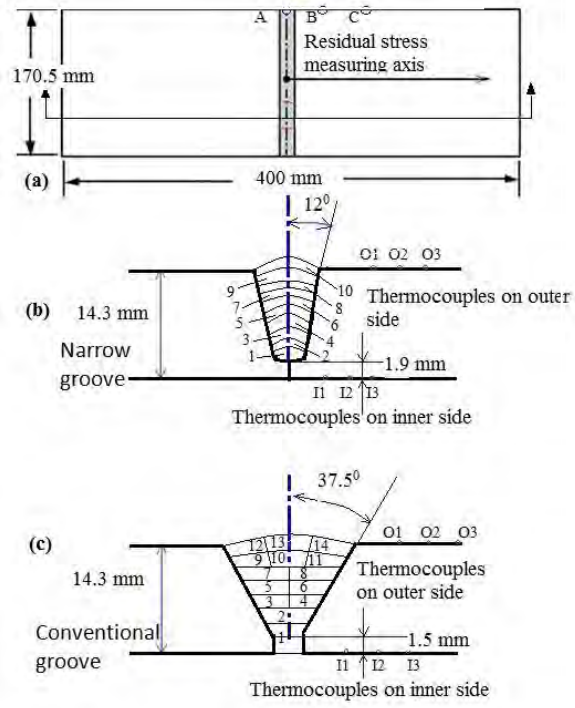

Figure 2: Schematic details for pipe weld joints of (a) Residual stress and temperature measurement for (b) Narrow groove and (c) Conventional V-groove

Table 2: Process Parameters

Bead on Plate						
Pass Number	Process	Diameter of filler rod (mm)	Voltage (V)	Current (A)	Wire Current (A)	Velocity (mm/min)
1	GTAW	2.4	13.5	160	0	63
GTAW with Narrow groove						
Root	GTAW	1.2	8.4	105	0	100
2	GTAW	1.2	8.4	105	15	110
3	GTAW	1.2	8.4	135	15	110
4	GTAW	1.2	8.4	140	15	100
5	GTAW	1.2	8.4	150	15	90
6	GTAW	1.2	8.4	145	15	90
7	GTAW	1.2	8.4	150	15	90
8	GTAW	1.2	8.4	145	15	90
9	GTAW	1.2	8.4	140	15	90
10	GTAW	1.2	8.4	150	15	90
GTAW with Conventional groove						
Root	GTAW	3.5	12	110	0	30
2	GTAW	2.4	12	110	0	35
3	GTAW	2.4	14	110	0	38
4	GTAW	2.4	14	120	0	45
5	GTAW	2.4	15	130	0	47
6	GTAW	2.4	15	130	0	46
7	GTAW	2.4	16	135	0	51

In case of pipe joints, temperature was measured at 6 locations as shown in Fig. 2. Three of six thermocouples were attached on the inner surface while remaining on the outer surface. Distance of thermocouple I1 from weld centreline was 4mm; I2 was about 7 mm, while I3 was at 10 mm from weld centre line. Thermocouples on the outer surface were at similar distance from the edge. Table 2 describes the process parameters in the welding processes used.

Residual stress Measurement

X-ray diffraction technique [8] was used for residual stress measurement for bead on plate. It exploits the fact that when a metal is under stress, applied or residual, the resulting elastic strains cause the atomic planes in the metallic crystal structure to change their spacing. X-ray diffraction can directly measure this inter-planar atomic spacing; from this quantity, the total stress on the metal can then be obtained. X-ray diffraction method employs Bragg's law to estimate the residual strains present in the atomic planes. In this method, a monochromatic X-ray beam of sufficient intensity is made to be incident on the atomic planes. The reflected beam from successive planes of atoms is observed. Bragg's law defines the condition for diffraction through the following equation:

$$n\lambda = 2d\sin\theta \quad (1)$$

Where, λ is the wave length of incident X-rays,

θ is the angle between the incident or reflected beam and the reflecting planes,

d is the interplanar spacing, and

n is the order of reflection

Equation (1) shows that, if the wavelength of X-rays is known, *d* can be determined by measuring the angle θ. In the presence of residual stresses, *d* changes, leading to a shift in X-ray diffraction peaks, which this is a measure of the residual stress. One of the main limitations of x-ray diffraction technique for residual stress measurement is depth of penetration. It is recommended that either the surface should be machined by electrochemical polishing or left as it is after welding. In our study, the surface was just cleaned by acetone. Incident x-ray beam should be perpendicular to the surface where residual stresses are to be measured. Curved bead surface makes it difficult to measure the stresses.

The Blind Hole Drilling Strain-Gauge (BHDSG) method [9] is an established technique for measuring residual stress used in case of pipe welds. Application of this method and calculation of residual stresses are discussed in [10]. Points of strain measurement are shown in the Fig.2. Strain gauges of the rosette type were mounted on the pipe at the selected points to measure the released strains after drilling in the centre point of the gauges by a very high-speed drill. After measuring the released strains by a strain indicator, the stresses in the axial and hoop directions were calculated. According to the following equations, based on the ASTM E837-92 standard:

$$_1 = \frac{_3(\mathrm{A}+\mathrm{B}\cos 2\ ) - _1(\mathrm{A}-\mathrm{B}\cos 2\ )}{4\mathrm{AB}\cos 2} \text{ and } \ _2 = \frac{_1(\mathrm{A}+\mathrm{B}\cos 2\ ) - _3(\mathrm{A}-\mathrm{B}\cos 2\ )}{4\mathrm{AB}\cos 2} \quad (2)$$

where,

$$\mathrm{A} = -\frac{1+}{2\mathrm{E}}\left(\frac{1}{\mathrm{r}^2}\right),\ \mathrm{B} = -\frac{1+\mu}{2\mathrm{E}}\left[\left(\frac{4}{1+\mu}\right)\frac{1}{\mathrm{r}^2} - \frac{3}{\mathrm{r}^4}\right],\ 2\beta = \tan^{-1}\left\{\frac{(\varepsilon_3+\varepsilon_1)-2\varepsilon_2}{(\varepsilon_3-\varepsilon_1)}\right\}$$

$$_1 = \ +90\ ,\ _2 = \ +45\ \text{ and } \ _3 =$$

ε_1, ε_2 and ε_3 are the released strain in the principal directions, respectively. E is Young's modulus, and ν is Poisson's ratio. Residual stresses were measured at points A, B and C as shown in Fig. 2. Point A is on weld centre-line while B and C were at 3mm and 7 mm respectively.

FINITE ELEMENT ANALYSIS

Thermal Analysis

Thermal analysis for all cases was done using three dimensional half models except for plate where quarter model was used as shown in Fig. 3. Eight noded brick elements were used in these models.

The energy balance between change in stored energy and heat flux leads to,

$$\mathrm{H} = \mathrm{Q} - \nabla\mathbf{q} \quad (3)$$

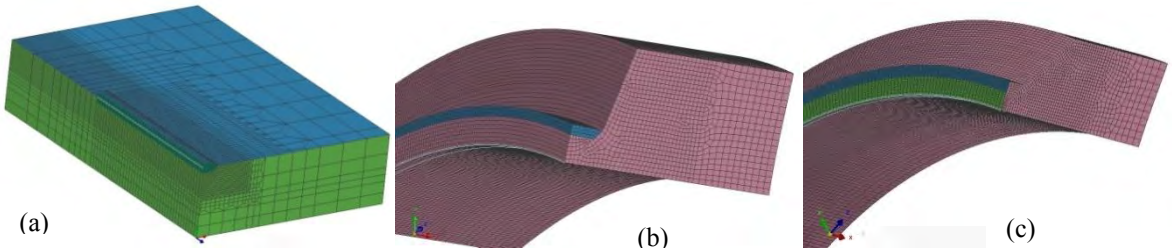

Fig. 3: Finite element model used for thermal analysis in case of: (a) Bead on Plate, (b) Narrow groove GTAW, (c) Conventional groove GTAW

where, Q (W/m^3) is the power per unit volume, is the density, H (J/m^3) is the volumetric enthalpy or heat content and q (W/m^2) is the heat flux vector.

Fourier's law for isotropic heat conduction gives

$$\mathbf{q} = -\mathbf{k}\nabla T \tag{4}$$

where k (W/m ^{0}C) or (W/m K) is the coefficient of conduction of given isotropic material.

The relations above can be combined to produce the classical heat conduction equation

$$\rho cT = Q + \nabla(K\nabla T) \tag{5}$$

The heat conduction equation, together with initial and boundary conditions, defines the thermal problem to be solved. Initial conditions were the ambient conditions. Convective and radiation heat losses are more complex boundary conditions for the outward flux. Then the flux depends on the temperature of the body and the surrounding and is written as

$$q_n = -k\nabla T \cdot \mathbf{n} = \frac{\partial T}{\partial \mathbf{n}} = h(T - T_\infty) + \epsilon\sigma(T^4 - T_\infty^4) \tag{6}$$

where, the first term is convective heat loss and h is the convective heat transfer coefficient.

At room temperature coefficient of convection was assumed to be 25 W/m^2. The second term is the heat loss due to radiation and is Stefan-Boltzmann's constant and is the emissivity factor. The latter is 1 for a perfect black body. The equation can be rewritten as

$$q_n = [h + \epsilon\sigma(T^2 + T_\infty^2)(T + T_\infty)](T - T_\infty) = h_{eff}(T - T_\infty) \tag{7}$$

where h_{eff} is effective coefficient of heat transfer

Double ellipsoidal heat source was used. The front half of the source is the quadrant of one ellipsoidal source, and the rear half is the quadrant of another ellipsoid. The power density distribution inside the front and rear quadrant is:

$$q_{f,r}(x,y,z) = \frac{6\sqrt{3}Qf_{f,r}}{abc_{f,r}\pi\sqrt{\pi}} \exp\left(\frac{-3x^2}{a^2} + \frac{-3y^2}{b^2} + \frac{-3[z+v(\tau-t)]^2}{c_{f,r}^2}\right) \tag{8}$$

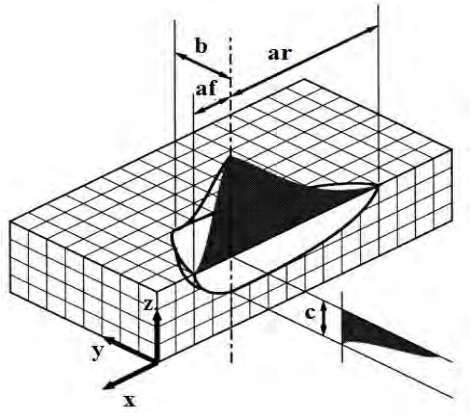

Fig. 4 Double Ellipsoidal Heat Source

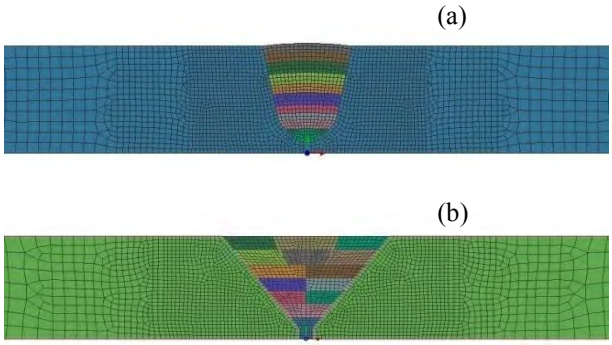

Fig. 5 Two dimensional axy-symmetry finite element model used in mechanical analysis for (a) Narrow groove (b) Conventional V-groove

Fig. 4 gives details of double ellipsoidal heat source. Parameters such as weld current, voltage, speed, arc efficiency and the size and position of the ellipsoids were specified. In pipe cases the weld pool size and shape were estimated from cross sectional metallographic data and from weld pool surface ripple markings. Input parameters of weld pool size were about 10% smaller than actual dimensions of weld pool which yielded into good agreement. Accurate results are obtained when the final computed weld pool dimensions were slightly larger than the ellipsoid dimensions [2]. This is easily achieved in a few iterations.

Mechanical Analysis

In case of bead on plate same model as that was used in case of thermal analysis was used. In case of pipe welds two dimensional axy-symmetry finite element models using four noded rectangular elements were used as shown in Fig. 5. Average thermal cycle obtained by thermal analysis imposed to obtain mechanical results.

An exact solution to a stress analysis problem satisfies three basic laws:

1. The conservation of linear momentum or the equilibrium equation,

$$\sigma_{ij,j} + \rho b_i = 0 \tag{9}$$

here, $_{ij}$ is the stress tensor and b_i is the body force. It is assumed that the stress tensor is symmetrical, i.e. $_{ij} = _{ji}$

2. The constitutive relation between stress and strain

$$[d\ ] = [D^{ep}][d\varepsilon] - [C^{th}]dT \quad (10)$$
$$[D^{ep}] = [D^{e}] + [D^{p}]$$

here $[D^e]$ is the elastic stiffness matrix, $[D^p]$ is the plastic stiffness matrix, $[C^{th}]$ is the thermal stiffness matrix, d is the stress increment, dε is the strain increment and dT is the temperature increment.

3. The compatibility relations between strain and displacements which is the conservation of mass must be satisfied.

$$\varepsilon_{ij,kl} + \varepsilon_{kl,ij} - \varepsilon_{lj,ki} - \varepsilon_{ki,jl} = 0 \quad (11)$$

In addition it satisfies two types of boundary conditions; the prescribed displacements or essential boundary conditions and the prescribed tractions or natural boundary conditions. A displacement FEM formulation was used to solve the constitutive, compatibility and equilibrium equations.

Material Modelling

Very low modulus of elasticity and yield stress same as that of the parent metal is assigned to the filler material. This results in transfer of strains from welded material to the material to be filled without generation of high stresses. Coefficient of expansion of filler material is neglected which ensures, no thermal stresses are generated in it.

Generally during the welding process, besides the plastic and thermal strains, the strain due to solid state phase transformation and creep potentially also give some contributions to the total strain. Because austenitic stainless steel 304L has no solid state phase transformation during cooling and the heating is relatively short, it can be expected that the strains contributed by phase transformation and creep can be neglected. The total strain increment at a material point can be summation of the elastic, plastic and thermal strain.

The parent and the weld material were assumed to have the same mechanical and thermal properties, as was provided in the software database for the material. The solidus temperature was 1360^0C, liquidus temperature was 1440^0C and the latent heat of fusion was 270KJ/Kg. Besides considering isotropic strain hardening behaviour annealing effect is also included in the numerical model. When the temperature of material at given point is higher than the annealing temperature, which was set 1300^0C the material will lose its hardening memory. The temperature dependent properties supplied with the software had been measured and tabulated by extensive experimentation.

RESULTS

Bead on Plate:

Experimental and numerical analysis result for residual stresses across weld bead in longitudinal and transverse direction have been shown in Fig. 6 and 7. From Fig. 6 (a), we can see that at start of the weld (line A) longitudinal residual stresses are tensile in nature and match well with that of the observation. Maximum stress of 155.7 MPa is observed on weld centreline against 170 MPa predicted by FEM. In Fig 6 (b) of transverse residual stresses are compressive in nature and match qualitatively with experimental observations on left side.

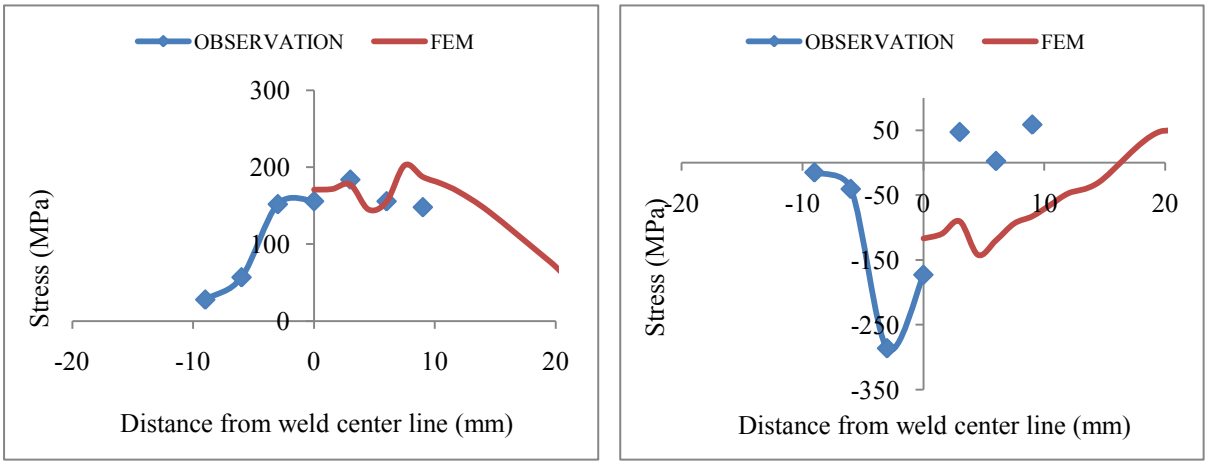

(a) (b)

Fig. 6 (a) Longitudinal and (b) Transverse stress at start of bead on plate

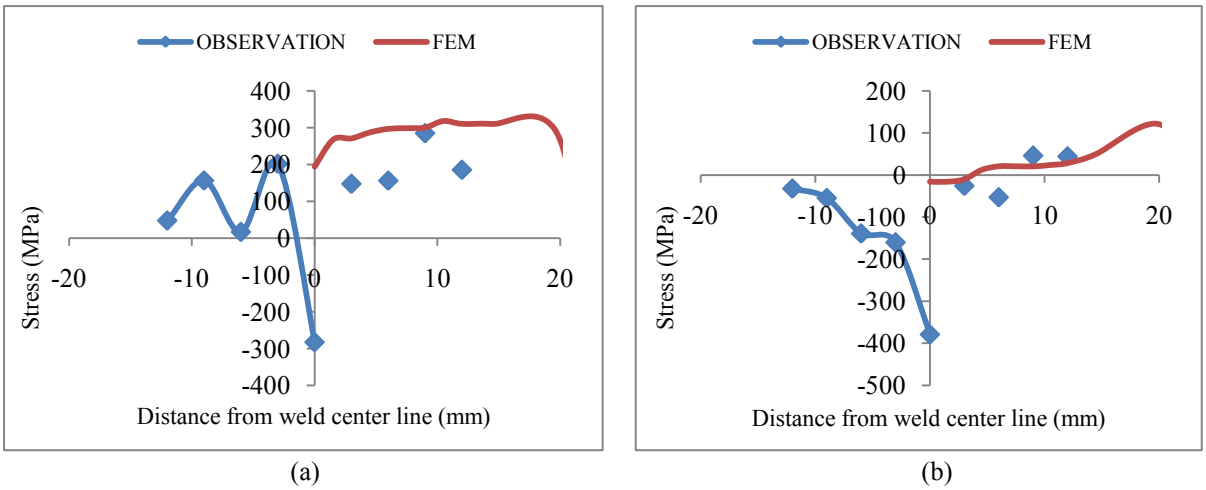

Fig. 7 (a) Longitudinal and (b) Transverse residual stress at middle of bead on plate

Fig. 7 shows distribution of Longitudinal and transverse stresses at middle of the weld bead (line B). Although stresses match qualitatively, major reason for the deviation is attributed to the limitation of the x-ray diffraction method, explained before.

GTAW with Narrow Groove:

Fig. 8 (a) shows thermal cycle predicted using FEM at 4 mm form weld centre line on inner surface of the weld joint using narrow groove. Peak temperature reached in root pass is 880^0 C. Peak temperature decreases with number of passes since distance of heat source from measured point increases with each pass. Fig. 8 (b) shows comparison of the observed thermal cycle with predicted for root pass at 4 mm from weld centre line on inner surface. Difference of about 100^0C is observed in peak temperatures which is attributed to the simplifications made in boundary conditions.

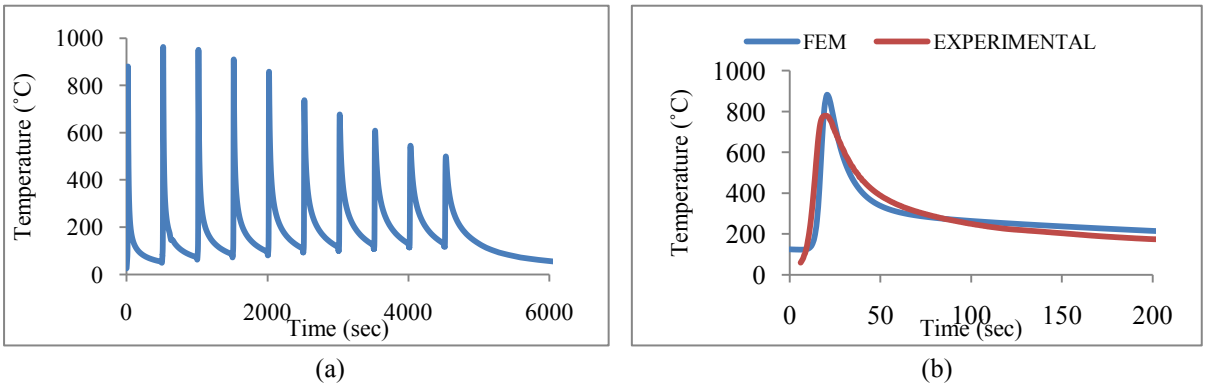

Fig 8 (a) Thermal cyle predicted using FEM analysis (b) Comparison of thermal cycle; at 4mm from weld centerline on inner surface

Resdiual stresses in case of weld joint using narrow groove are tabulated as shown in Table 3. Hoop and axial residual stresses match qualitatively. On outer surface of weld joint using narrow groove which match qualitatively. Residual stresses by FEM are overprdicted than experimental observation except for hoop stress on outer side.

Table 3 Residual stresses in weld joint using Narrow Groove on inner surface

Distance from weld centre line (mm)	Hoop stress (MPa)		Axial stress (Mpa)	
	FEM	EXPERIMENT	FEM	EXPERIMENT
On inner Surface				
0	406.0	263.22	169.1	162.15

Distance from weld centre line (mm)	Hoop stress (MPa)		Axial stress (MPa)	
	FEM	EXPERIMENT	FEM	EXPERIMENT
6	389.0	112.88	177.9	45.167
10	261.1	95.411	192.0	16.025
16	0.768	365.76	156.2	130.83
On outer surface				
0	45.448	279.456	-275.328	-80.022
3	40.655	294.851	-277.058	203.637
7	70.134	321.364	-288.805	160.584

GTAW with Conventional Groove:

Fig. 9 (a) shows thermal cycle prdicted using FEM at 4 mm form weld centre line on inner surface of the weld joint using conventional V-groove. Peak temperature reached in root pass is 1200^0 C. Peak temperature decreases with number of passes since distance of heat source from measured point increases with each pass. Fig. 9 (b) shows comparison of the observed thermal cycle with predicted for root pass at 4 mm from weld centre line on inner surface.

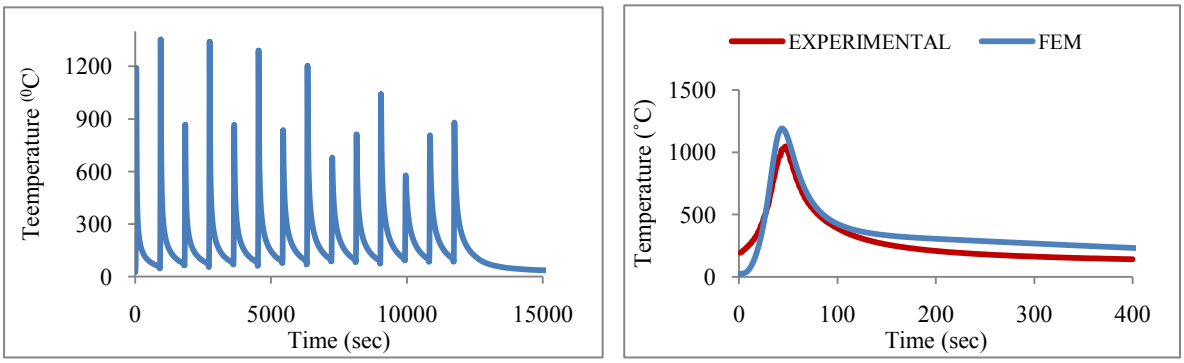

(a) (b)

Fig. 9 Thermal cycle at 4 mm from weld centerline on inner surface (a) predicted using FEM (b) comparison using FEM and experimental observation

Resdiual stresses in case of weld joint using conventional groove on the inner surface are tabulated as shown in Table 4. Hoop and axial residual stresses match qualitatively.

Table 4 Residual stresses in weld joint using Conventional V-Groove on inner surface

Distance from weld centre line (mm)	Hoop stress (MPa)		Axial stress (Mpa)	
	FEM	EXPERIMENT	FEM	EXPERIMENT
0	571.984	341.713	538.195	275.631
3	543.227	228.906	558.702	155.704
7	536.689	342.906	574.868	344.492

Comparison of GTAW with Narrow Groove and Conventional Groove:

Fig. 10 shows comparison of residual stresses in pipe weld using Narrow groove with Conventional groove. As can be seen, residual stresses in fusion zone (FZ) and heat affected zone (HAZ) for conventional groove are greater than narrow groove since heat input in previous is almost three folds which results in higher thermal gradient. On inner surface of the pipe as shown in Fig. 10 (a) all stresses were found to be tensile in FZ and HAZ. All of these are balanced by the subsequent compressive stresses about 25 mm or more away from

weld centerline. On outer surface of the pipe as shown in Fig. 10 (b) only hoop stress in case of Narrow groove is tensile in nature in FZ and HAZ. Axial stresses are compressive in FZ and HAZ.

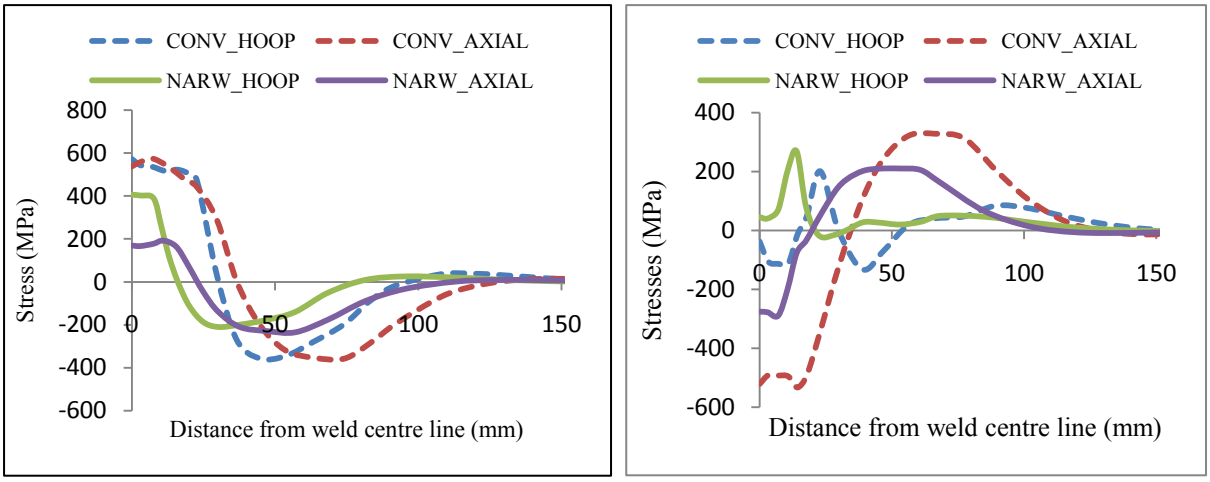

(a) (b)

Fig. 10 Residual stresse predicted using FEM on (a) inner surface and (b) outer surface

CONCLUSION:

This paper summerizes numerical and experimental methods for the prediction and measurment of temperature and residual stresses in the pipe weld joints.

Peak temperature is marginally over predicted where as heating an cooling rate compare well. It indiactes that temperature distribution can be well predicted using FEA.

Hoop and axial residual stress at ther weld root could be predicted well using FEA but there is significant difference in case of weld top. Effort is requird to find out the deficiencies either in measurement or analysis.

REFERENCE:

[1] Rosenthal D., "The theory of moving sources of heat and its applications to metal treatments", Transactions ASME, vol. 68, 849, 1946

[2] Goldak J., Chakravarti A. and Bibby M. A finite element model for welding heat sources, Metallurgical Transactions B, Vol. 15B, pp 299-305, June 1984

[3] B. Brickstad, B. L. Josefson, "A parametric study of residual stresses in multi-pass butt-welded stainless steel pipes", International Journal of Pressure Vessels and Piping, vol 75, 1998, pp.11-25

[4] Dean Deng, Hidekazu Murakawa, Wei Liang, "Numerical and experimental investigations on welding residual stress in multi-pass butt-welded austenitic stainless steel pipe", Computational Material Science, vol 44, 2008, pp. 234-244

[5] Dean Deng, Hidekazu MurakawaY., "Finite element analysis of temperature field, microstructure and residual stress in multi-pass butt-welded 2.25Cr–1Mo steel pipes", Computational Material Science, vol 43, 2008, pp. 681-695

[6] M. C. Smith, A. C. Smith, "Part 1:NeT bead-on-plate round robin: Comparison of transient thermal predictions and measurements", International Journal of Pressure Vessles and Piping, vol 86, 2009, pp. 96-109

[7] M. C. Smith, A. C. Smith, "Part II: NeT bead-on-plate round robin: Comparison of residual stress predictions and measurements", International Journal of Pressure Vessles and Piping, vol 86, 2009, pp. 79-95

[8] Norton JT. X-ray determination of residual stress. Material Evaluation, February 1973;21A

[9] Measurement of residual stresses by blind hole drilling method; Measurement Group (TN-503)